GPPS-NA-2018-0071

NUMERICAL LOSS BREAKDWOWN STUDY FOR A SMALL SCALE, LOW SPECIFIC SPEED SUPERCRITICAL CO2 RADIAL INFLOW TURBINE

Joshua A. Keep
Queensland Geothermal Energy Centre of Excellence
University of Queensland
j.keep @uq.edu.au
St Lucia, Queensland, Australia

Ingo H. J. Jahn
Centre for Hypersonics
University of Queensland
i.jahn@uq.edu.au
St Lucia, Queensland, Australia

ABSTRACT

Radial inflow turbines, characterised by a low specific speed are a candidate architecture for the supercritical CO_2 Brayton cycle at small scale, i.e. less than 5MW. Prior cycle studies have identified the importance of turbine efficiency to cycle performance, hence well designed turbines are key in realising this new cycle. With operation at high Reynolds numbers, and small scales, it is uncertain as to the relative importance of loss mechanisms in supercritical CO_2 turbines.

This paper presents a numerical loss breakdown study of a low specific speed radial inflow turbine operating on supercritical CO_2. A combination of steady-state and transient calculations are used to determine the source of losses within the turbine stage. Losses are compared with preliminary approaches. Geometric variations to address high loss regions of stator and rotor are trialled.

Analysis shows stage losses to be dominated by endwall viscous losses in the stator when utilising stator geometry definitions derived from gas turbines. These losses are more significant than predicted using preliminary methods. A reduction in stator-rotor interspace and use of a foiled blade showed a significant improvement in stage efficiency, without detriment to stator-rotor interaction. An investigation into rotor blading shows favourable performance gains through the inclusion of splitter blades. Through these modifications, a stage performance improvement of 7.5 points is possible over the baseline design.

INTRODUCTION

Thermal power conversion cycles, using supercritical carbon dioxide (sCO_2) were first proposed by Angelino (1968). Benefiting from the non-linear thermo-physical properties of sCO_2, these cycles achieve thermodynamic efficiencies better than comparable steam Rankine cycles at temperatures above 500-600^{0}C as shown by Dostal (2004).

With appropriate cycle enhancements, and consideration of realistic component performance, cycle efficiencies in excess of 50% can be attained, with the ability to maintain acceptable turndown performance (Jahn and Keep, 2017). Further benefits of the supercritical fluid are high densities and low viscosities, which results in compact and power dense components.

In Australia, the Australian Solar Research Institute (ASTRI) is investigating concentrated solar thermal power in conjunction with thermal energy storage with the sCO_2 power cycle. The aim of this program is to develop a power generation technology that addresses energy despatchability at a competitive cost in the 1-25MW range, as a solution to provide electricity to rural communities (ASTRI 2012). A number of other sCO_2 power system demonstration projects are currently under way in the USA (Held 2014; Moore et al., 2015; Wilkes et al., 2016). For applications in this power range, specific speeds in the range 0.2 to 0.6 are typical and radial turbomachinery is a preferred solution (Balje 1962).

Recent works have shown that cycle efficiency is more sensitive to turbine efficiency than compressor efficiency (Brun et. al, 2017), hence it is clear that design efforts should be focused on improving the performance of the turbine. In order for efficient turbines to be realised, an understanding of their internal loss mechanism is vital.

Present preliminary turbine design methodologies utilise loss models developed for gas turbines. Whilst some of these are physics based and should provide satisfactory performance with a change in fluid, others are empirical or experience based. In order to enhance preliminary design, and hence speed up the design process, it is necessary to verify preliminary methods for new applications and update models where appropriate.

Two recent studies (Wheeler and Ong, 2014; Pini et al., 2017) use steady-state and transient CFD calculations to

elucidate loss mechanisms in Organic Rankine cycle (ORC) turbines. Wheeler and Ong (2014) shows discrepancies between CFD calculations and a typical preliminary method, particularly in the proportional loss split between stator and rotor.

Whilst the turbines of previous numerical studies on ORC turbines utilise similarly dense fluids and operate at a similar scale and specific speed to those of sCO_2, some key differences are that ORC machines operate with fluids with low acoustic speed, high volumetric flow variation and higher pressure ratios. Hence these turbines cannot be considered similar according to similitude theory as presented by White and Sayma (2015).

In the present paper, a numerical loss breakdown study is performed for a low specific speed 300kW sCO_2 radial inflow turbine.

METHODOLOGY

The present turbine design is based on conservative supercritical CO_2 cycle conditions with a target shaft power of 300kW. Design constraints are listed in Table 1.

Table 1: Stage operating conditions

$P_{o,in}$ (MPa)	20
$T_{o,in}$ (K)	833
Rotational Speed (RPM)	50000
$P_{o,in}/P_{exit}$ (-)	2.2
Mass flow rate (kg/s)	3.0
Power (kW)	300

Based on these cycle constraints, preliminary radial inflow turbine designs are assessed using the TOPGEN meanline design software (Ventura et al., 2012; Qi et al., 2017; Reddell et al., 2016) with a search space defined by non-dimensional head (Ψ) and flow (Φ) coefficients. The ranges used are $0.1 < \Phi < 0.55$ and $0.5 < \Psi < 2.5$. In addition to operating constraints, both tip clearance and incidence loss models are tuned. The relative tip clearance of candidate designs exceeds the typical validity limits of the tip clearance loss model within TOPGEN. As an alternative, tip clearance loss is modelled as a fixed 10% penalty to total to static efficiency based on simulations of sCO_2 turbines of similar design (Meijboom, 2017).

The number of rotor blades (Zr) is set at 16 based on packaging constraints at the rotor exit. Incidence losses were modelled with $\beta_{4,opt} = -25^o$ according to the relationship with blade number presented by Whitfield (Whitfield, 1990). Rotor blading is constrained to a purely radial inlet.

In addition to the above modelling assumptions, rotor radius ratio and meridional velocity ratio were tuned to reduce the exit flow angle. The radius ratio is set at $R_{6h}/R_4 = 0.2$ whilst the meridional velocity ratio is set as $C_{m6}/C_{m4} = 1.5$.

The selected design has flow coefficient, stage loading coefficient and a predicted efficiency of $\Phi = 0.1$, $\Psi = 1.0$ and $\eta_{t,s} = 83.61$ %. The jet speed ratio (ν) approximately corresponds to that of maximum total to static efficiency for the given specific speed presented by Rohlik (1968). Additional parameters are summarised in Table 2, with nomenclature following conventions outlined by Baines in Moustapha et al. (2003).

Table 2: Preliminary turbine performance and geometric parameters

ns (-)	0.146
Λ (-)	0.58
ν (-)	0.64
R_4 (mm)	60.19
b_4 (mm)	1.85
R_{6H} (mm)	12.04
$R_{6S\ (mm)}$	26.39
α_4 (^{o})	81.5
β_6 (^{o})	-73.64
Zs	21
Zr	16

Stator design

Considering the stator exit flow is subsonic, monotonic converging, un-cambered blading is used with circular trailing and leading edges. Blade solidity (C/S) and radial spacing ($R_{2,TE}$ / R_4) is defined using the values proposed by Simpson et al. (2013). Subject to a fixed flow angle (α_4), blade setting angle (α_{b4}) is determined iteratively using a design tool (Keep, 2017), with flow angle (α_4) determined using the modified cosine rule for radial inflow blading proposed by Ricardo (Hiett and Johnston, 1963). Stator geometry is summarised in Figure 1 and Table 3.

Table 3: Stator geometric parameters

T_{LE} (mm)	4.0
T_{TE} (mm)	0.5
C/S (-)	1.25
$R_{2,TE}$ / R_4 (-)	1.175
α_{b4} (^{o})	84.5

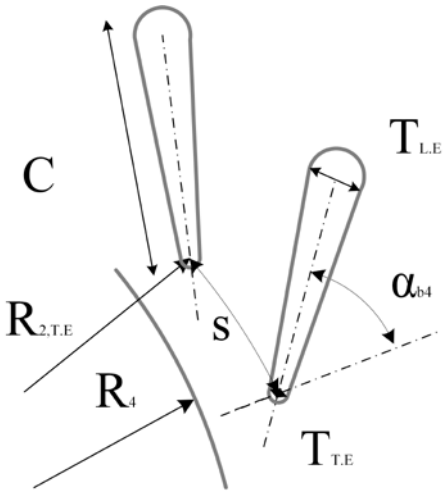

Figure 1: Stator geometry definition.

Rotor design

The rotor geometry is defined through a combination of meridional passage curves and blade wrap angle subject to a

purely radial inlet (no sweep or lean) and pre-defined outlet blade angle.

The meridional passage definition follows a similar approach to Glassman (Glassman, 1976), whereby the shroud and hub lines are defined by circular and elliptical sections respectively. For the present case, the shroud line is extended in the axial direction with a 10 mm linear section. The

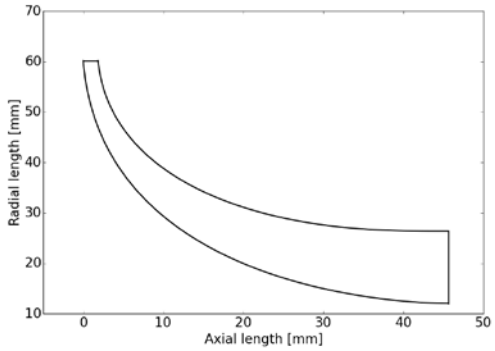

Figure 2: Meridional passage definition of rotor.

meridional passage is shown in Figure 2. Blade angle is defined through wrap angle definition at the hub. The blade exit angle is constrained to the value predicted by the deviation model within TOPGEN as β_{6bH} = -63.4 °. Wrap angle was benchmarked from an early NASA study (Kofskey and Nusbaum, 1972) on the influence of turbine specific speed on turbine performance, where high wrap angles were characteristic of rotor geometries designed for low specific speed. The use of a large wrap angle has the desirable effect of smoothing the passage quasi-orthogonal area distribution (see Figure 4.) when highly tangential exit flows are required, as with the present application. A value of 100° is selected for wrap angle, while wrap angle distribution was set visually similar to production turbines subject to blading

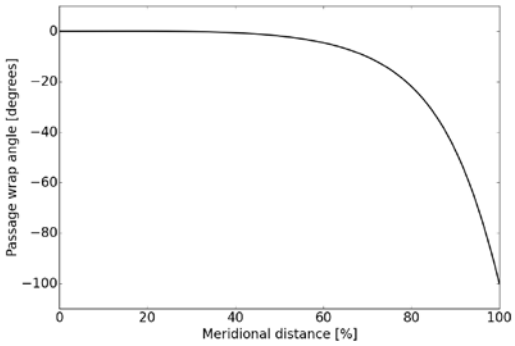

Figure 3: Blade wrap angle distribution of rotor.

constraints. The wrap angle distribution for the hub of the turbine is illustrated in Figure 3.

Blading thickness is set at a constant 1.0 mm, with a rounded trailing edge and square leading edge. Tip clearance is set to 0.3 mm for both axial and radial clearance on the shroud of the impeller based on minimum values proposed by TOPGEN (Ventura et al., 2012), and checked against anticipated tolerance stackup.

Numerical model

The turbine Stage is modelled as single passage for the stator and rotor, without diffuser or inlet delivery system. Geometry is constructed using ANSYS BladeGen, with a hexahedral mesh created using ANSYS TurboGrid.

Steady-state, transient blade row, and transient stage simulations are conducted using the ANSYS CFX 18.1 solver (ANSYS, 2017). The Reynolds-averaged Navier-Stokes (RANS) equations are closed with SST k-ω turbulence model.

The inlet flow to the stator is modelled with a flow angle to match stator blading. The inlet flow is assumed to be fully turbulent, and modelled with a turbulence intensity of 5 %. For steady state simulations, rotor and stator domains are coupled using a mixing plane interface based on stage average velocity. Rotor blading is modelled from the rotor inlet radius (R_4), with a gap of 1% of the rotor inlet radius at

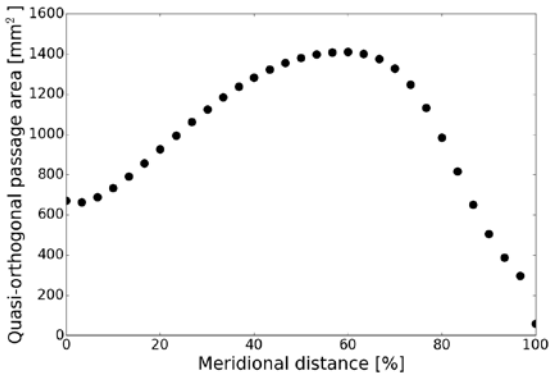

Figure 4: Quasi-orthogonal passage area schedule.

the inlet of the rotating domain. Shroud tip clearance is modelled, with the gap between the rotor blade and shroud surface meshed with equal spacing to the shroud and blade boundary. The shroud surface is modelled as non-rotating. An exit block of 10mm axial length is added to the rotor mesh to minimise the influence of boundary conditions on the region of interest.

sCO_2 specific thermodynamic and transport properties are incorporated into the CFD solver through the use of a user generated lookup table for CO2, with properties sourced from CoolProp (Bell et al., 2014). The lookup table is sized at 200 x 200 and spans the range of 7.5 < P < 22 MPa and 700 < T < 950K.

Second order numerical schemes are used for turbulence and advection. Solutions were deemed to be converged when rms residuals for mass, momentum, and turbulence had reduced by at least 5 orders of magnitude.

First layers within the mesh are sized to retain y+ in the desired range of 30 < y+ < 300 for the wall functions used by the selected turbulence model (ANSYS, 2017). Grid dependence of the solution is assessed using steady state simulations based on total to static expansion efficiency of the stage. Three grids are assessed, with total to static expansion efficiency for each shown in Table 4. Based on the less than 0.05 percentage points difference between the

nominal and fine meshes, the nominal mesh is selected for further calculations. The selected mesh is composed of approximately 619K nodes in the rotor, and 265K nodes in the stator.

Table 4: Total to static efficiency for different mesh sizes.

Nodes ($x10^3$)	497	884	1707
$\eta_{t,s}$ (%)	73.11	73.50	73.58

For transient calculations, a time step study is conducted for a single blade passage, matching all other relevant parameters with the steady state case. The nominal time step is set at 30 time steps per blade pass, similar to that selected in several recent studies for subsonic stages using the same solver (Simpson et al., 2013; White and Sayma, 2015). Solution convergence is assessed based on blade torque, where solutions are considered converged when variation in torque is less than 0.05% between blade passes. Once converged, solutions for each time step value are compared on the basis of total to static machine efficiency computed from time and flux averaged quantities time averaged for one rotor revolution. Further to transient calculations for a single

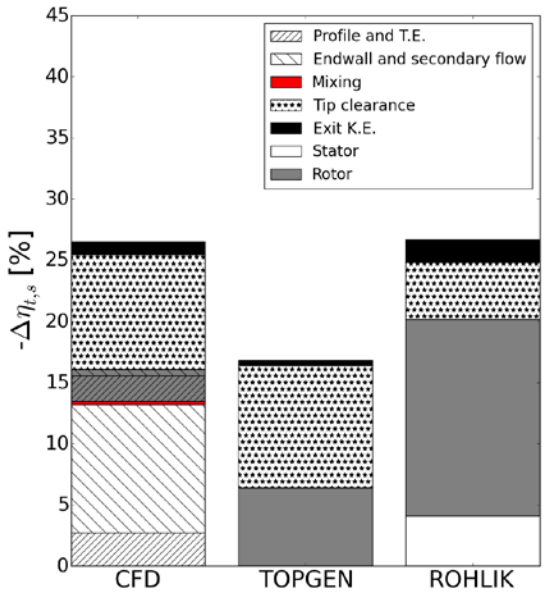

Figure 5: Breakdown of loss contributions to efficiency.

passage, a full stage is also considered for the nominal time step. Results for the time step study are shown in Table 5. Owing to the small variation when compared to steady-state and when compared to the full stage simulation, a single blade passage with time step corresponding to 30 time steps per blade pass is selected for transient calculations.

Table 5: Time step study for unsteady simulations. Efficiency compared to nominal steady state solution.

Model / time step (per blade pass)	**$\Delta\eta_{t,s}$ (Percentage points)**
Single passage / 10	-0.26
Single passage / 30	-0.13
Single passage / 100	-0.22
360^0 / 30	-0.16

RESULTS AND DISCUSSION

To assess performance of the turbine stage, a loss breakdown study is performed. CFD Losses are calculated based on proportional entropy rise and presented as an efficiency deficit in Figure 5. Entropy losses are determined following the method of Wheeler and Ong (2014) as follows.

Profile and trailing edge loss is determined as the entropy rise over each component due to blade boundary layer and trailing edge losses, with the absence of endwall shear (i.e. through setting a slip-wall boundary condition on the shroud and hub surfaces). Endwall and secondary flow losses are determined as the proportional entropy rise over each component resulting from viscous endwall effects and

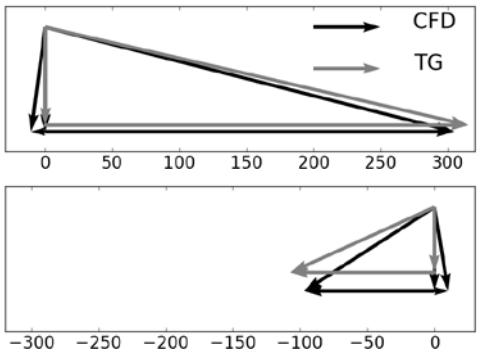

Figure 6: Inlet and outlet velocity triangles for CFD and TOPGEN.

induced secondary flow. Tip clearance loss is considered in a similar manner for the rotor. Mixing loss is determined from the entropy rise across the mixing plane in steady-state calculations. Stator/rotor interaction is determined as the difference in efficiency between unsteady and steady calculations. For the present geometry this difference is small at less than 0.2 percentage points. For clarity stator/rotor interaction losses are not shown in Figure 5. More detail is given on this in the following section on stator loss breakdown.

Comparing predicted losses with those estimated in the meanline design method, TOPGEN, losses are under predicted. A clear discrepancy is the stator, which is not included in the loss calculation of TOPGEN, as with many other preliminary methods for use in gas turbine design (Moustapha et al, 2003). For those applications the loss incurred in the stator is typically small, and does not impact stator outlet velocity, and hence rotor performance estimation. For the present turbine, this is not the case, and is clearly illustrated in the turbine velocity triangles at inlet and outlet in Figure 6. The magnitude of absolute velocity entering the rotor is in good agreement between design and simulation, however the observed discrepancy in exit absolute velocity is due to the underestimation in total enthalpy losses by TOPGEN, and how this is accounted for in the outlet area calculation.

In contrast to the stator, rotor losses are overestimated compared to CFD. A likely cause for this is are lower relative velocities within the rotor than what is used in the TOPGEN loss calculation.

A further comparison is made with data presented by Rohlik (1968) for a *ns*=0.155 radial inflow gas turbine. Compared to this rotor effects are over-estimated, whilst stator effects are underestimated. It is likely that some discrepancy can be attributed to differences in stator and tip clearance dimensions.

Stator

As observed in Figure 6, the absolute flow angle at the rotor is not sufficiently tangential. In the design of the stator, the blade setting angle was determined according to the cosine rule (Hiett and Johnston, 1963). To investigate the effectiveness of this method, flux averaged absolute flow angle is plotted against normalised radial distance in the stator-rotor interspace in Figure 7.

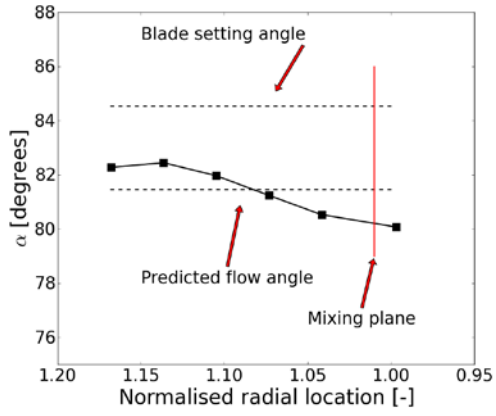

Figure 7: Absolute flow angle variation in stator-rotor interspace.

Figure 7 shows the flow angle initially exceeds the predicted value, then the flow turns radially inwards. This turning is likely due to the larger viscous effects acting in the tangential direction owing to the highly tangential blade setting angle and tangential velocity. I.e. absolute flow angle at the rotor inlet is a function of path travelled, which is a function of stator radius ratio and blade setting angle range. Based on this observation, it would appear that the cosine rule provides a reasonable estimate of flow angle at within +/- 2 ° of the desired flow angle for the present geometry. For further improvements in prediction accuracy, a more detailed study of the interspace is required to correlate for a range of setting angles and interspace sizes.

Losses within the stator are investigated through a streamwise plot of flux averaged entropy rise in Figure 8.

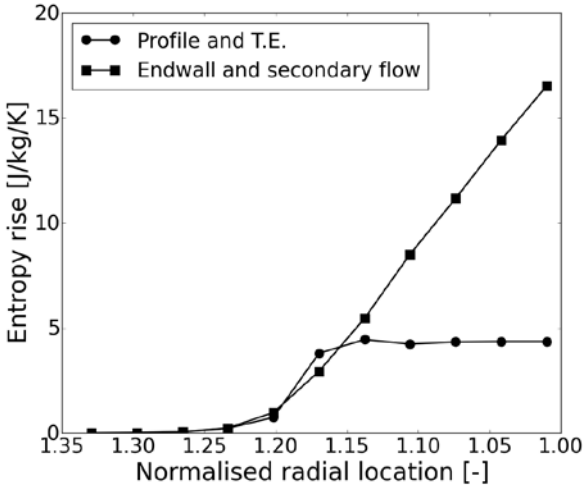

Figure 8: Stator entropy rise as a function of streamwise distance from inlet.

The two sources of entropy rise are determined in the same manner as for the efficiency based loss breakdown for the stage.

Examining entropy generation due to profile and trailing edge mixing, entropy rise occurs early in the stator domain, and plateaus following the blade trailing edge (located at 1.175) . This suggests that the profile loss is more significant than trailing edge mixing losses.

For the current work, an un-optimised straight blade profile is used, and the profile losses account for approximately 20% of the entropy rise within the stator, making this a major area for improvement. Losses due to blade profile are however overshadowed by endwall losses, which are approximately three times greater. Figure 8. shows that endwall losses increase beyond blading (trailing edge at 0.5). As there is little secondary flow within the stator, this entropy increase can be attributed to viscous friction on the endwalls due to the higher Mach number flows in the region between stator trailing edge and rotor. As trailing edge losses in the stator, and mixing losses between stator and rotor (see Figure 5.) are low, adjusting the dimensions of the interspace is an effective way to increase performance.

Stator-rotor interspace sizing

To assess the impact of modifying the stator-rotor interspace, performance is assessed in terms of stator entropy rise (The sum of endwall and profile + trailing edge losses) and stator-rotor interaction (composed of mixing and

unsteady interaction). To investigate unsteady stator-rotor interactions, unsteady calculations are performed for a single passage. The performance impact of stator-rotor interaction is determined as the difference in total to static stage efficiency between steady-state and transient simulations, as in the study of Wheeler and Ong (2014).

The original stator geometry spacing of $R_{2,TE}$ / R_4 = 1.175 was sized based on a recent gas turbine study of Simpson et al. (2013). Earlier experimental studies, as

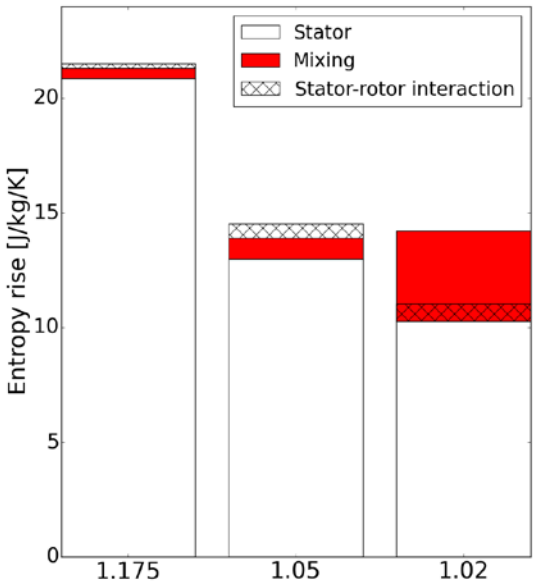

Figure 9: Comparative loss breakdown of stator stator designs by interspace ($R_{2,TE}$ / R_4) size.

summarised in that study, and in Moustapha et al. (2003), detail efficient designs of a more compact geometry, some with $R_{2,TE}$ / R_4 ~ 1.04. To determine if stator losses can be minimised through reducing stator-rotor interspace, stator

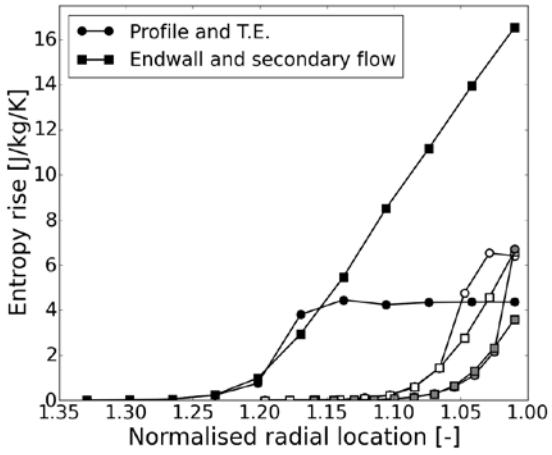

Figure 10: Stator entropy rise as a function of streamwise distance from inlet. Unfilled symbols correspond to $R_{2,TE}$ / R_4 = 1.05, grey symbols for $R_{2,TE}$ / R_4 = 1.02 design.

designs with $R_{2,TE}$ / R_4 = 1.05 and 1.02 are assessed.

Figure 9 shows a comparative loss breakdown for the three designs. From this breakdown, it appears that more compact stator designs are beneficial for stage aerodynamic performance due to the significant reduction in entropy rise over the stator, and small increase in mixing and stator-rotor interaction.

Examining the $R_{2,TE}$ / R_4 = 1.02 case in more detail, the unsteady simulation yields a higher efficiency than the steady state solution. This would tend to imply an overestimation of mixing losses by the mixing plane used in steady state calculations. In Figure 9, mixing and stator-rotor interactions determined from the transient solution are shown by the red hatched region, whilst the entire red region is representative of the losses calculated from the steady state solution.

For further verification of the root cause, Figure 10 shows a comparison of entropy rise for interspace geometries. Note that the contribution of end wall losses is reduced as interspace size is reduced.

It would appear beneficial from an efficiency standpoint to reduced interspace sizing to $R_{2,TE}$ / R_4 = 1.02, however the impact of additional forcing on the rotor blades should be adequately assessed against rotor blade fatigue risk prior to moving beyond traditional gas turbine limits (Whitfield and Baines, 1990). This assessment is beyond the scope of the present work.

Considering the $R_{2,TE}$ / R_4 = 1.05 case, total to static machine efficiency (assessed with steady state simulations) improves by 3.9 percentage points over the baseline case.

Stator blading

As an alternative to further reductions in interspace size, the impact of stator blade profile is investigated. The combined losses in the stator for the $R_{2,TE}$ / R_4 = 1.05 case are appreciable at approximately 30% of total machine losses, and Figure 10 indicates that approximately half of those within the stator can be attributed to the blade profile and trailing edge wake.

In contrast to the simple profile used for prior calculations, a foiled blade profile is investigated. For the design of subsonic axial turbine stages, Schobeiri (Schobeiri, 2011) recommends a turbine blade thickness profile with thickness distribution resembling a NACA-0015 foil. To assess the impact of this blade design, a new geometry was created with the new thickness distribution applied to the $R_{2,TE}$ / R_4 = 1.05 stator design, whilst retaining solidity and setting angle.

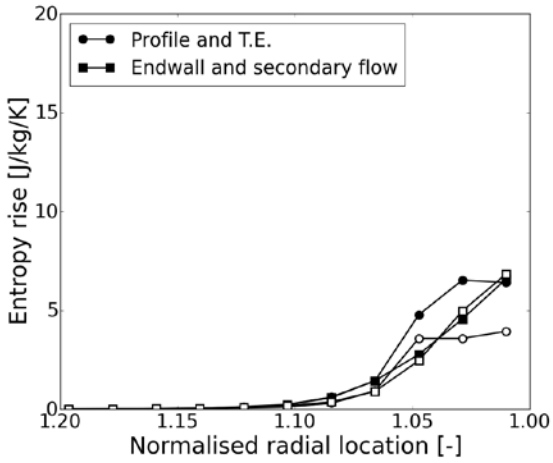

Figure 11: Stator entropy rise as a function of streamwise distance from inlet. Unfilled symbols correspond to foiled blade.

For an initial comparison, entropy rise over the stator is investigated in Figure 11, which shows a significant difference in entropy rise beyond the trailing edge. Further to entropy rise, pressure distribution over the blade surface is investigated in Figure 12. The new foiled blade geometry demonstrates a much smoother pressure distribution, particularly on the suction side of the blade. Furthermore, the pressure distribution of the foiled blade conforms to the design guidelines suggested by Schobeiri, which prescribe an almost zero pressure gradient with no sign change over the first 60-70% of the blade chord, followed by a strong acceleration over the remainder of the blade (Schobeiri, 2011). Considering total to static machine efficiency, the use of a foiled blade results in an additional 1.2 percentage point increase in performance.

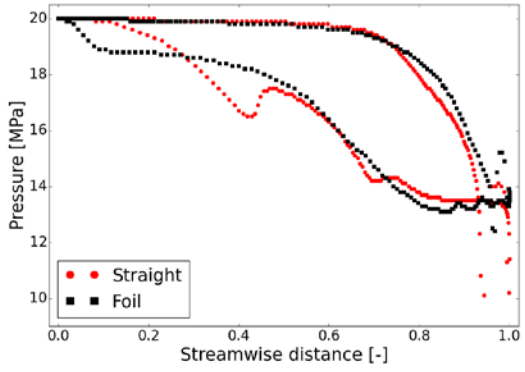

Figure 12: Pressure distribution of stator blades.

As a further comment on this blade profile, visual comparison with production turbines indicates that this blade design (or very similar) is commonly used. One such application being the APU turbine presented by Jones (Jones, 1996).

Rotor

Overall, the CFD predicted losses within the rotor are less than those predicted by preliminary methods. A potential causal factor for this is that the relative velocity within the passage remains very low. Figure 13 illustrates blade surface Mach numbers. Note that the Mach numbers of the blade suction surface dip towards mid span. This dip in Mach number may be a potential causal factor for TOPGEN overestimating rotor losses, as TOPGEN assumes a weighted mean of velocities for determining viscous losses within the rotor. Comparing these blade loadings to those presented in an early NASA study into low specific speed turbines of similar geometry, it is clear that the surface Mach numbers of the present turbine do not represent an optimised case. A likely root cause for this is drop in Mach number at approximately 50% Meridional distance is the peak in quasi-orthogonal schedule (see Figure 4.) that is coincident with the dip in Mach number. This peak in area schedule is a direct result of the highly tangential exit flow blade angle used in conjunction with circular / elliptical endwalls. A recent study into optimisation of an ORC turbine (Pini et al., 2017) presented a rotor design comparison that shifted from a rotor with flow separation regions with circular / elliptical endwall definitions, to an optimised rotor with a modified hub contour shifted towards the shroud line. This shift in hub contour causes a reduction in blade height and available flow area, which is expected to smooth the quasi-orthogonal area schedule.

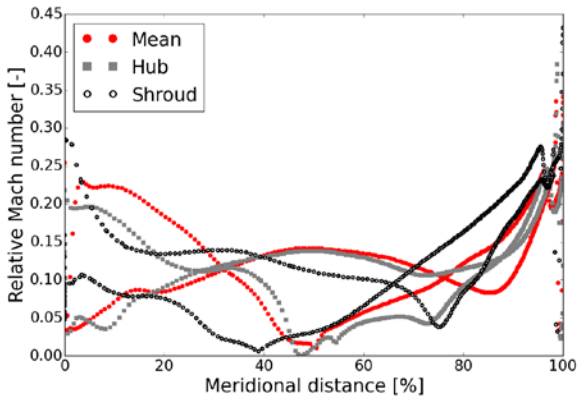

Figure 13: Rotor blade surface Mach number. Hub and shroud taken as 0.1 and 0.9 span respectively.

While it is clear that there is opportunity to improve the rotor blade loadings and quasi-orthogonal area schedule for the passage through variation in hub contour and wrap angle distribution, the overall contribution of rotor internal losses to stage efficiency still remains small at approximately 3 percentage points. With regard to magnitude of losses, a more important consideration is tip clearance losses. Tip clearance losses in radial turbines are dominated by flows in the tip gap towards the exit of the rotor (Dambach et al., 1998). Modification to the rotor hub endwall towards rotor exit may be used to shift the high momentum stream on the shroud surface towards the hub, and hence reduce tip clearance flows and losses at the rotor exit.

While losses in the rotor are proportionally small, it is uncertain as to whether the rotor is operating at it's optimum jet speed ratio (ν) or incidence. The preliminary design of the turbine is based around the recommended optimal value for ν, and incidence loss based on a correlated value of $\beta_{4,opt}$ for the number of blades. It is important to note that incidence loss is a non-physical loss model, and that optimal incidence varies with secondary flow, which is a function of the number of rotor blades. Whitfield places this in the range $-40^o < \beta_{4,opt} < -20^o$, with less incidence required when more blades are used (Whitfield, 1990).

Optimal rotor blade number can be determined according to several criteria. Early methods set minimum blade number according to the limit of inlet recirculation based on incompressible flow and an assumed velocity profile. Using The Jamieson relation (summarised in Whitfield, 1990), the optimum number of blades for the present inlet conditions is Zr=42. This method leads to an overestimation for gas turbines due to higher viscous losses and packaging problems associated with a large number of blades (Whitfield and Baines, 1990). In light of these constraints, an updated criteria for gas turbines was proposed by Glassman, which for the present design yields Zr=20 (Glassman, 1976).

Recall that the current design is set at Zr=16 based on blade packaging constraints at the rotor outlet. An alternative means to increase blading at the rotor inlet is through the use of splitter blades. To assess the impact of the number of rotor blades on stage performance, two additional geometries are considered which employ splitter blades extending 65% of the meridional passage. The two geometries are Zr = 12, and Zr = 16, both with a matching set of splitter blades, corresponding approximately to the Glassman case of Zr=20, and the limiting geometric case respectively. Off-design efficiency characteristics of these geometries are compared with the nominal 16 blade rotor geometry. Rotors are used in conjunction with the $R_{2,TE} / R_4 = 1.05$ straight blade stator. Identical mesh density is used for the new geometries, with additional cells used to mesh the splitter blade surfaces. Steady-state calculations are used to determine the trend in total to static efficiency in the range ν = 0.3 to 0.9.

Figure 14 shows the predicted efficiency trends for the three turbine geometries. Both geometries utilising splitter blades show an efficiency improvement over the original rotor geometry at the design speed. Performance improvements are 1.2 and 2.4 percentage points for the 12 and 16 blade rotors with splitter blades respectively. Of the points trialled, peak efficiency occurs at the design jet speed velocity ratio for all geometries. All three turbines feature similar off-design performance, which is in line with that presented in the early study of Hiett and Johnston (1963). The principle difference is in off-design performance at high shaft speed, where rotors with higher blade counts suffer larger losses.

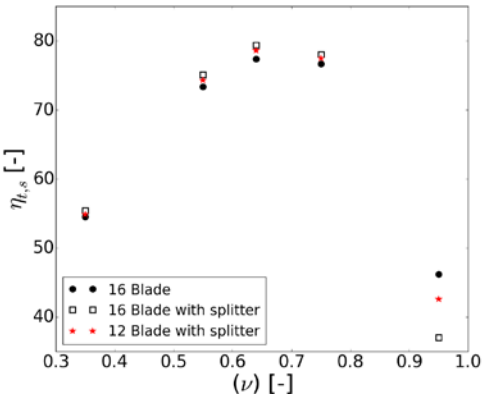

Figure 14: Total to static efficiency as a function of jet speed ratio (ν) for different rotor geometries.

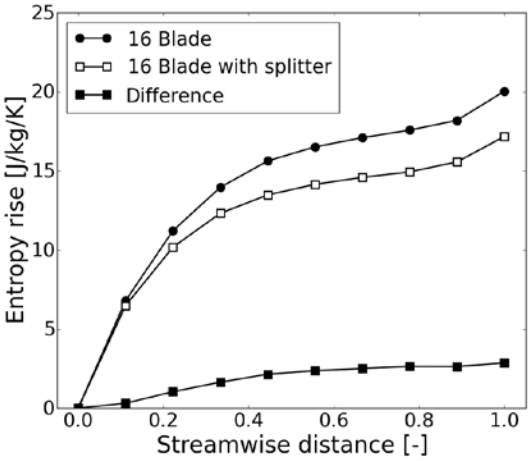

Figure 15: Rotor entropy rise as a function of streamwise distance from inlet.

Considering the observed correlation between efficiency at design conditions and blade number, a potential reason for improvement is reduction of secondary flows within the inlet of the passage due to reduced span between blades. To verify this, entropy rise over the rotor passage is compared for the 16 blade geometries with and without splitter blades in Figure 15. Figure 15 shows that the primary difference in entropy rise between the two geometries occurs at less than 0.5 streamwise distance. This would imply that for the current design that secondary flows induced within the inlet region of the rotor due to incidence on low blade count rotors are more significant than viscous blade losses incurred on high blade count rotors at the design speed.

CONCLUSIONS

In this paper, a numerical loss breakdown study into a low specific speed radial inflow turbine operating on sCO_2 is presented. The loss breakdown of the initial geometry reveals higher than anticipated losses within the stator and interspace. These losses are attributed to endwall viscous losses within the interspace. Evaluating geometries with different interspace sizing using unsteady CFD calculations reveals that these losses can be reduced through reducing the extent of the interspace to $R_{2,TE} / R_4 = 1.05$ without significant impact on stator-rotor interactions. Future work should focus on quantifying the impact of further interspace reductions through structural vibration analysis.

Profile losses within the stator were of the same order of magnitude to the rotor, at approximately 3 points efficiency penalty to the stage. Through the use of a thickness profile approximating a NACA-0015 foil, these losses were halved This suggests that this profile should be used in lieu of a simple un-cambered linear thickness profile. Analysis of the rotor inlet absolute flow angle showed that the cosine rule appropriately accounts for flow deviation and provides a suitable estimate for blade setting angle.

Analysis of rotors with different blade numbers shows enhanced efficiency for higher blade count rotors. Doubling the number of blades at the rotor inlet increased stage efficiency by 2.4 points at the design shaft speed. Investigation reveals that for the current stage conditions secondary flow effects at the inlet are more significant than viscous losses to overall performance. The use of splitter blades is a suitable means to provide additional inlet blading with a constrained outlet passage area.

To streamline the design process, meanline tools need to adequately determine stage geometry and predict performance. Based on the present work, the following changes are suggested for low specific speed sCO_2 turbines:

- For the stator, the cosine rule should be implemented to predict stator blade setting angle, owing to the large deviation between setting and flow angles.
- The stator/rotor interspace should be sized with $R_{2,TE} / R_4 = 1.05$.
- With small interspace sizing and the use of a foiled blade, the total losses in the stator will be below the magnitude at which they have a significant influence upon the rotor geometry determination. Alternatively, a mean path friction model should be used to appropriately account for stator losses.
- Rotor blade number should be set in an automated manner to be the maximum obtainable within the constraint of packaging at the rotor exit.

Overall, steady and unsteady CFD calculations revealed that modifications to the interspace gap, stator blade profile, and rotor blade number enable a low specific speed radial inflow turbine stage operating with sCO_2 to achieve an efficiency in excess of 81%. This is approximately 7.5 points higher than if the stage was designed using existing design rules for gas turbines.

NOMENCLATURE

α – Flow angle in the absolute frame [degrees]
b – Blade height [mm]
β – Flow angle in the relative frame [degrees]
Λ – Degree of reaction [-]
ns – Specific speed [-]
ν - Jet speed ratio [-]
Z – Number of blades [-]

Subscripts

0 – inlet, stagnation
2 – stator blade exit
4 – rotor inlet
6 – rotor outlet
b – blade
H - hub
LE –leading edge
R - rotor
S – shroud, stator
TE – trailing edge

ACKNOWLEDGMENTS

This research was supported by the Australian Solar Thermal Research Institute (ASTRI), a project supported by the Australian Government.

REFERENCES

[1] Angelino G. (1968). Carbon Dioxide Condensation Cycles for Power Production. Journal of Engineering for Power 90 (3) 287-295.
[2] ANSYS (2017). CFX solver theory guide 18.1. Retrieved January 2018. support.anays.com
[3] ASTRI (2012). Australian Solar Thermal Research Initiative. www.astri.org.au
[4] Balje O.E. (1962). A study on Design Criteria and Matching of Turbomachines: Part A – Similarity Relations and Design Criteria of Turbines, Journal of Engineering for Power, Jan 1962, 83-102
[5] Bell I.H., Wronski J., Quoilin S., Lemort V. (2014). Pure and pseudo-pure thermophysical property evaluation and the open-source thermophysical property library coolprop. Industrial & engineering chemistry research, 53(6):2498
[6] Brun K., Friedman P., Dennis R. (2017). Fundamentals and Application of Supercritical Carbon Dioxide (sCO_2) Based Power Systems. Woodhead Publishing, ISBN:978-0-08-100804-1
[7] Dambach R., Hodson H., and Huntsman, I. (1998). An experimental study of tip clearance flow in a radial inflow turbine. In ASME 1998 International Gas Turbine and Aeroengine Congress and Exhibition. American Society of Mechanical Engineers.
[8] Dostal V. (2004). A Supercritical Carbon Dioxide Cycle for Next Generation Nuclear Reactors, PhD thesis, Massachusetts Institute of Technology
[9] Glassman A.J. (1976). Computer program for design analysis of radial-inflow turbines. NASA Technical Note. NASA-TN-D-8164
[10] Hiett G.F., Johnston I.H. (1963). Paper 7: Experiments concerning the aerodynamic performance of inward flow radial turbines. In Proceedings of the Institution of Mechanical Engineers, Conference Proceedings, volume 178, pages 28
[11] Held T.J. (2014). Initial test results of a MegaWatt-class supercritical CO_2 heat engine. In: 4th International sCO_2 Power Cycle Symposium, Pittsburgh, PA.
[12] Jahn I., and Keep J. (2017). On the off-design performance of supercritical carbon dioxide power cycles. Proceedings of Shanghai 2017 GPPF. GPPS-2017-0049.
[13] Keep J. (2017). Radial inflow turbine nozzle guide vane design tool. Mechanical Engineering Technical Report 2017/18. School of Mechanical and Mining Engineering, The University of Queensland.

[14] Kofskey M.G., and Nusbaum W.J. (1972). Effects of specific speed on experimental performance of a radial-inflow turbine. NASA Technical Note. NASA-TN-D-6605
[15] Meijboom, L. (2017). Development of a turbine concept for supercritical CO_2 power cycles, Master thesis, Delft University of Technology.
[16] Moore J., Brun K., Evans N., Kalra C. (2015). Development of a 1 MWe supercritical CO_2 test loop. In: Proc. ASME Turbo Expo GT2015-43771, Montreal, Canada.
[17] Moustapha H., Zelesky M., Baines N., and Japikse D. (2003). Axial and radial turbines. Concepts NREC. ISBN 0-933283-12-0.
[18] Pini M., De Servi C., Burigana M., Bahamonde S., Rubino A., Vitale S., and Colonna P. (2017). Fluid-dynamic design and characterization of a mini-ORC turbine for laboratory experiments. Energy Procedia 129, 1141-1148. doi:10.1016/j.egypro.2017.09.186
[19] Qi J., Reddell T., Qin K., Hooman K., Jahn J. (2017) Supercritical CO2 Radial Turbine Design Performance as a Function of Turbine Size Parameters. ASME. J. Turbomach. 139(8. doi:10.1115/1.4035920.
[20] Reddell T., Ventura C., Rowlands A., Qi J., Jacobs P., and Jahn I. (2016). TOPGEN: Radial Inflow Turbine Model - Userguide and Example Book, Engineering Report, School of Mechanical and Mining Engineering, University of Queensland.
[21] Rohlik H. (1968). Analytical determination of radial inflow turbine design geometry for maximum efficiency. NASA Technical Note. NASA-TN-D-4384
[22] Schobeiri, M.H. (2011). Turbomachinery flow physics and dynamic performance. Springer, ISBN: 978-3-642-24674-6.
[23] Simpson A., Spence S., Watterson J. (2013). Numerical and Experimental Study of the Performance Effects of Varying Vaneless Space and Vane Solidity in Radial Turbine Stators. ASME. J. Turbomach. 135 (3). doi:10.1115/1.4007525.
[24] Ventura C., Jacobs P., Rowlands A., Petrie-Repar P. and Sauret E. (2012). Preliminary design and performance estimation of radial inflow turbines: An automated approach. Journal of Fluids Engineering, 134(3).
[25] Wheeler A.P., and Ong J., (2014). A study of the three-dimensional unsteady real-gas flows within a transonic ORC turbine. ASME Paper No. GT2014-25475.
[26] White M. and Sayma A. (2015). The application of similitude theory for the performance prediction of radial turbines with small-scale low temperature organic Rankine cycles. Journal of Engineering for Gas Turbines and Power 137(12).
[27] Whitfield, A. (1990). The preliminary design of radial inflow turbines. Journal of Turbomachinery 112(1).
[28] Whitfield A., Baines N.C. (1990). Design of radial turbomachines. Longman Scientific & Technical, ISBN: 978-0582495012.
[29] Wilkes J., Allison T., Schmitt J., Bennett J., Wygant K., Pelton R., Bosen W. (2016). Application of an integrally geared compander to an sCO_2 recompression Brayton cycle. In: The 5th International Symposium – Supercritical CO_2 Power cycles, San Antonio, TX.